Journal of Molecular Graphics and Modelling 38 (2012) 375–381

Contents lists available at SciVerse ScienceDirect

Journal of Molecular Graphics and Modelling

journal homepage: www.elsevier.com/locate/JMGM

New statistical boundary conditions for argon–tungsten interactions

M.S. Ozhgibesov[a,*], T.S. Leu[a], C.H. Cheng[a], A.V. Utkin[b]

[a] Department of Aeronautics and Astronautics, National Cheng Kung University, Tainan 701, Taiwan, ROC
[b] Khristianovich Institute of Theoretical and Applied Mechanics SBRAS, Novosibirsk, Russia

ARTICLE INFO

Article history:
Accepted 26 June 2012
Available online 7 July 2012

Keywords:
Molecular dynamics
Maxwell distribution
Argon–tungsten interactions
Morse potential
Statistical analysis
Boundary conditions

ABSTRACT

In this study, scattering processes of argon beam impinging on tungsten surface are investigated numerically by applying molecular dynamics (MD) simulations. Energy transfer, momentum change, and scattering processes of argon gas atoms from W(1 1 0) surface are discussed. A new model of argon–tungsten (Ar–W) interaction is proposed. Based on the new proposed model, one can simplify the boundary conditions of this problem. The new boundary conditions are proved to be in line with previous experimental and theoretical results. This paper demonstrates how to proceed normalization and further conversion of the MD simulation results into boundary conditions. Application of the new proposed boundary conditions for Ar–W interactions provides a significant speedup of computations.

1. Introduction

Nowadays a lot of micro/nano systems become an integral part of our daily life, for example: gravity sensor or micro gyroscope are applied in many handheld electronic gadgets. Recent technological advances allowed one to create micro/nano devices with characteristic size of several nanometers. The design processes of such micro/nano devices are very expensive and complicated and involve both experimental and numerical studies of solid and fluid mechanics inside the device. It should be noted that micro/nano flow is characterized by a high degree of rarefaction. It means that assumption of classical continuum theory cannot be applied for analysis of micro/nano flow. Fortunately there is a numerical method, called molecular dynamics (MD) simulation method. It is based on the fundamental principles of mechanics and allows one to simulate processes on molecular level, i.e., the simulated system is considered as ensemble of molecules, rather than a continuous medium.

One of the most challenging parts of numerical simulations of a micro/nano flow is boundary conditions on the solid–liquid interface. The choice of boundary conditions (BC) influences on a flow significantly [1]. The incorrect BC might cause the wrong estimation of fluid behaviors in a micro/nano system. There are two ways to set up the BCs for the MD simulations: (1) to represent the solid parts of the simulated system by molecular structures and consider interactions between fluid molecules and solid boundary molecules; (2) to use relationships which state dependence between parameters of fluid molecule impinged on the solid boundary and the scattered one. The first approach is the most comprehensive one, but one should realize it also increases the number of simulated molecules significantly. Consequently the time of computations rises as well. The second way is widely used due to its relative simplicity. The most commonly used model [1–3] is specular-diffusive model proposed by Maxwell [4] in his studies of gas–surface interactions. The key point of Maxwell's BC is that a gas molecule impinging on a surface is scattered into two fractions, one that reflects specularly and exchanges no energy and the other that accommodates completely and desorbs with an equilibrium distribution corresponding to the surface temperature. Maxwell's BC was extensively used for studies of gas flow through microchannels. Recently we have shown [5] that this specular-diffusive model is too rough to reproduce all the processes accompany the interactions of argon molecules with tungsten substrate.

The energy transfer and other processes accompanying the scattering of rarefied gases from solid surfaces have been the subject of a series of studies. Weinberg and Merrill [6] determined angular distributions for gas atoms scattered by a single-crystal W(1 1 0) surface. The experimental results of Janda et al. [7] allowed the researchers to relate the average kinetic energy of scattered argon atoms to the surface temperature, as well as to the incident kinetic energy. The theoretical explanations for argon atoms scattering from a self-assembled monolayer on Ag(1 1 1) have been proposed recently by Fan and Manson [8]. Furthermore, Gibson et al. [9] conducted a detailed study of Ar scattering from an ordered 1-decanethiol–Au(1 1 1) monolayer. Recently, Chase et al. [16] have conducted experimental and molecular dynamics studies of argon

* Corresponding author. Tel.: +886 6 2757575x63638; fax: +886 6 2389940.
E-mail address: omiser@gmail.com (M.S. Ozhgibesov).

1093-3263/$ – see front matter.
http://dx.doi.org/10.1016/j.jmgm.2012.06.013

scattering from liquid indium. They have shown how the angular and energy distributions of scattered atoms depend on incident energy. Inapplicability of the simple hard-sphere model for the description of gas–surface interactions is also presented.

While there are many publications related to gas–surface interactions, their results are still insufficient to define boundary conditions that can describe the gas flow in micro/nano systems. The best way to study gas–surface interactions is to conduct an experiment, but one should realize that accurate measurements of gas–surface interactions on a microscopic level are very expensive and time consuming. Fortunately, the recent achievements in computer science and numerical methods made it possible to investigate such processes using MD simulation method.

In this paper, MD method was applied to study the argon gas scattering processes on a W(1 1 0) surface. This approach made it possible to precisely describe the interaction between argon gas and tungsten. The aims of this work were to study effects of argon scattering on the tungsten surface and to propose boundary conditions describing correlations between the parameters of incident and scattered atoms. The method applied in the present paper can be simply expressed as the bombardment of a tungsten surface with argon atoms, where further analysis of the scattered atoms' trajectories was conducted. Analysis of both angular distributions and distributions of velocities of scattered atoms were performed using mean values and root mean square deviations (RMSDs). The combinations of these parameters provide complete information about process of gas atoms scattering process. It is shown that results of current study are in line with experimental and theoretical results obtained by the other researches. The information obtained in simulations was statistically analyzed and represented by polynomial functions of incident energy and angle of incidence. All the functions that state relationship between parameters of impinging gas atoms and scattered atoms have been obtained using the Least Squares Method (LSqM). As a conclusive step of the work, we have proposed an algorithm describing an implementation of the relations mentioned above to a real study of gas flow with tungsten boundary. These relations can be used to specify boundary conditions for argon–tungsten interactions. The main result of this work is proposed new boundary conditions which are able to reproduce mechanism of argon–tungsten interactions and allow one to significantly reduce computation time required for the studies of gas flow around metal surface.

2. Methodology and computation

The physical system investigated in this study consisted of tungsten W(1 1 0) substrate with a temperature of T_{surf} and argon atoms with an initial velocity vector magnitude V^i and velocity vector direction determined by the azimuthal (in horizontal plane) and polar (in vertical plane) angles α^i and β^i, respectively. The simulation procedure consisted of a substrate bombardment of argon atoms, after which the scattered atoms' parameters V^s, α^s, and β^s were determined, as shown in Fig. 1.

Current research was performed numerically by using MD simulation method. All algorithms described in this study were implemented using Fortran code developed by the authors of this paper. In order to evaluate the gas scattering effects, different collimated beams of argon atoms with intensity of $2{\cdot}10^5$ Pa are set up to impinge on the (1 1 0) face of a tungsten crystal. The interactions among tungsten atoms were taken as being sums of pairwise Morse potential:

$$\Phi_{W-W} = \begin{cases} D_W[e^{-2B_W(r-R_W)} - 2e^{-B_W(r-R_W)}], & 0 < r < 2.3R_W \\ 0, & r \geq 2.3R_W \end{cases}, \quad (1)$$

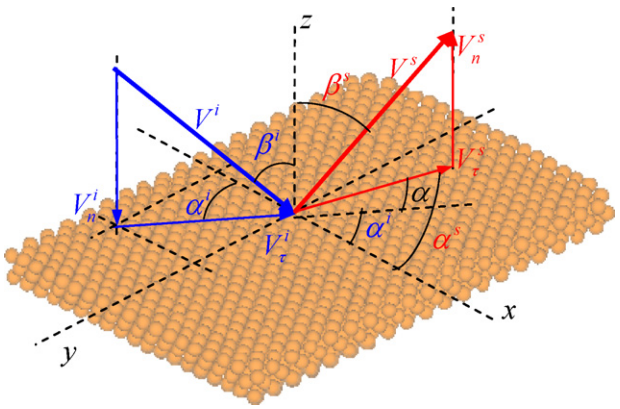

Fig. 1. Coordinate system, where α^i and β^i are the incident azimuthal and polar angles, respectively; α^s and β^s are the scattered atom's azimuthal and polar angles, respectively; $\alpha = \alpha^S - \alpha^i$ are the azimuthal angle change caused by the scattering of gas atom; V^i_n and V^i_τ are the normal and tangential velocity components of the incident atom; V^S_n and V^S_τ are the normal and tangential velocity components of the scattered atom.

where the potential's parameters [10] were: $D_W = 0.9906$ eV, $B_W = 14.116\ nm^{-1}$, $R_W = 0.3032$ nm.

To describe the interaction between both argon–tungsten and argon–argon atoms, Lennard–Jones potential functions are applied and depicted as following:

$$\Phi_{W-Ar} = \begin{cases} 4\varepsilon_{WAr}\left[\left(\frac{R_{WAr}}{r}\right)^{12} - \left(\frac{R_{WAr}}{r}\right)^{6}\right], & 0 < r < 2.5R_{WAr} \\ 0, & r \geq 2.5R_{WAr} \end{cases}, \quad (2a)$$

$$\Phi_{Ar} = \begin{cases} 4\varepsilon_{Ar}\left[\left(\frac{R_{Ar}}{r}\right)^{12} - \left(\frac{R_{Ar}}{r}\right)^{6}\right], & 0 < r < 2.5R_{Ar} \\ 0, & r \geq 2.5R_{Ar} \end{cases}, \quad (2b)$$

where the parameters values used for the case of argon–tungsten and argon–argon, respectively, were: $\varepsilon_{WAr}/k_B = 25.17$ K, $R_{WAr} = 2.93$ Å and $\varepsilon_{Ar}/k_B = 119.18$ K, $R_{Ar} = 3.4$ Å.

The initial lateral position for the impinging atom was selected randomly on a plane 17 Å above the average position of atoms of the uppermost solid layer. In order to model the scattering of a velocity-selected, collimated beam, the initial momentum of the incident atom was taken to be the same for each trajectory of a given set. The second order velocity Verlet scheme [10,11] with time step of $\Delta t = 10^{-16}$ s (smaller than the characteristic time of atom interactions) was used for an integration of equations of motion. The computational process was continued until all the gas atoms were within the force field of the tungsten atoms. Scattered gas atoms that went beyond this distance were excluded from the system (argon atoms did not pass through the tungsten substrate), and information on their velocities and coordinates were stored in a file. The exclusion of these scattered atoms reduces the time required for the calculation and prevents the randomization of velocities of argon atoms as a consequence of their collision with each other.

3. Results and discussion

This study was performed for a wide range of initial parameters of the impinging beam and metal surface as well. Total of 1920 cases were computed. The current investigations were conducted for various angles of incidents (from $\beta^i = 0$–70° with 5° steps), a series of surface temperatures ($T_{surf} = 350$ K, 400 K, 450 K, 500 K), and varied velocities of impinging Ar atoms (from $V^i = 100$–1600 m/s with 50 m/s steps).

Any analytical or numerical study based on mathematical descriptions has assumptions and simplifications. Consequently,

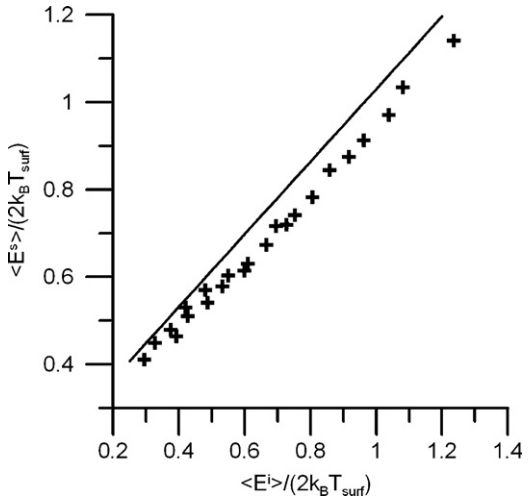

Fig. 2. Mean energy of scattered atoms versus energy of impinging atoms at $\beta^i = 45^\circ$.

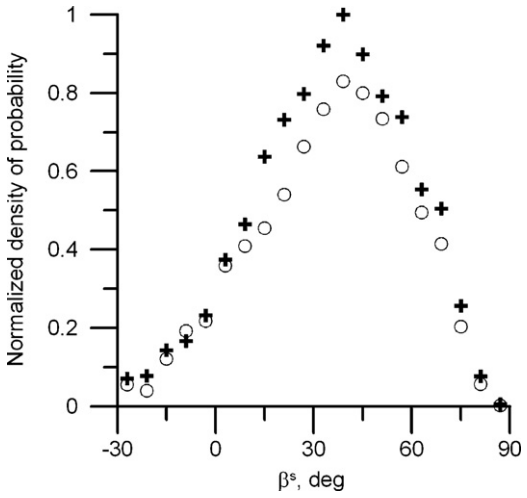

Fig. 3. Angular distribution of normalized probability density function in case of Ar scattering from W(1 1 0) at $T_G = 295$ K and incident angle $\beta^i = 45^\circ$. +, $T_{surf} = 500$ K; ◯, $T_{surf} = 350$ K.

results of such works must be compared with related experimental results in order to prove the reasonability of assumptions. Fig. 2 shows the correlation of the mean kinetic energies of the impinging atoms (initial energy of the beam) with the mean kinetic energy of the beam scattered (average energy of scattered atoms) by the tungsten surface. Solid line in Fig. 2 is the result from Janda experiments [7] and black cross symbols represent MD results obtained in the current study. Both results show the linear relationship between the mean kinetic energies of the impinging atoms and mean kinetic energy of the scattered atoms when the angle of the incidents was $\beta^i = 45^\circ$. The linear relationship from MD results can be fitted by the following function:

$$\langle E^s \rangle = b_B \langle E^i \rangle + b_S (2k_B T_{surf}), \tag{3}$$

where k_B is the Boltzmann's constant, and $b_S = 0.18$ and $b_B = 0.77$ are the proportionality factors.

The difference between the Janda experimental data and the MD simulation results does not exceed 9%. This difference can be explained by the fact that even the best MD models are a rough approximation of real processes. For example, the simulated substrate was ideal, i.e., it had no irregularities or scratches, while real substrate may have some faults. Based on the above, we conclude that achieving 9% difference is a reasonable result.

Another important parameter of the gas–surface interaction is the momentum change of the atoms, which can be characterized by an angular distribution of scattered atoms. Fig. 3 illustrates the normalized distributions of probability density of the polar angle of the scattered atoms (normalization was carried out by the peak value in order to improve visibility). Circles and crosses correspond to two cases of surface temperature, $T_{surf} = 350$ K and $T_{surf} = 500$ K, respectively. Furthermore, the temperature and incident angle of the argon beam were equal to $T_G = 295$ K and $\beta^i = 45^\circ$, respectively. As can be seen, the argon scattering distribution peaks increased in intensity with the increase of surface temperature. This finding is in line with the results of Weinberg [6].

Fig. 4 shows the average energy of the scattered beam as a function of incident beam energy $\langle E^i \rangle$ for different values of the incident angle β^i of the beam. It is clear that all plots presented in Fig. 4 have two regions: (1) a linear region, where the mean energy of the scattered atoms linearly depended on the incident energy; and (2) a nonlinear region, corresponding to relatively low energies of impinging Ar atoms. The linearity of dependence between $\langle E^s \rangle$ and $\langle E^i \rangle$ can be clarified by using correlation coefficient presented in Table 1.

If the distribution of random numbers corresponded to a Maxwell–Boltzmann distribution, the relationship between root-mean-square deviation (RMSD) σ and the mean value μ would be described by the following relation (see e.g., [12]):

$$\frac{\sigma}{\mu} = \frac{1}{2}\sqrt{\frac{3\pi - 8}{2}} \approx 0.42 \tag{4}$$

The ratio (σ_V/μ_V) of RMSD to the mean velocity of the atoms scattered by the surface as a function of both incident beam energy and incident polar angle is presented in Fig. 5. One can see that the value of σ_V/μ_V approaches 0.42 (shown in Eq. (4)) with decreasing incident energy regardless of the incident polar angle β^i, i.e., the distribution of velocities of scattered argon atoms tends towards a Maxwell–Boltzmann distribution. A similar effect was mentioned by Fan and Manson [8] and observed experimentally in Section 2 of Ref. [15] and in Section 3.D of Ref. [16]. The more detailed description of the methodology and method of analysis can be found in the previous work [5].

Correlation between average energy of scattered atoms and parameters of incidence was approximated using the least square method (this method was used to obtain all approximation func-

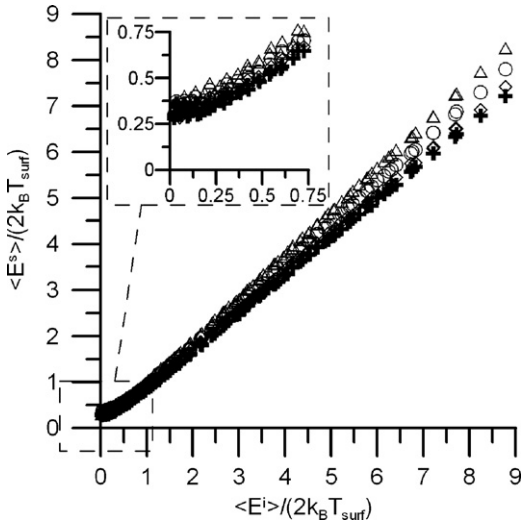

Fig. 4. Mean energy of scattered atoms versus energy of impinging Ar atoms. +, $\beta^i = 0^\circ$; ◇, $\beta^i = 20^\circ$; ◯, $\beta^i = 40^\circ$; Δ, $\beta^i = 60^\circ$.

Table 1
Correlation coefficients between $\langle E^i \rangle$ and $\langle E^s \rangle$ for different angle of incidence β^i.

β^i	0°	5°	10°	15°	20°	25°	30°	35°
Correlation coefficient	0.999437	0.999431	0.999467	0.999439	0.999435	0.999452	0.999453	0.999389
β^i	40°	45°	50°	55°	60°	65°	70°	
Correlation coefficient	0.999429	0.999468	0.999478	0.999499	0.999486	0.999549	0.999626	

tions discussed in current work). Eq. (5) represents the dependence between $\langle E^s \rangle$, E^i, and β^i. It should be noted, that the units of E^i and β^i are Joule and degree, respectively.

$$\left\langle E^s \right\rangle = f(E^i, \beta^i) = E^i \cdot \underbrace{\sum_{k=0}^{3} A0_k \cdot (\beta^i)^k}_{b_B} + (2k_B T_{surf}) \cdot \underbrace{\sum_{k=0}^{5} B0_k \cdot (\beta^i)^k}_{b_S}, \tag{5}$$

where b_S and b_B have the same physical meaning as in Eq. (3).

Coefficients $A0$ and $B0$ in Eq. (5) depend on polar angle β^i and their values are shown in Table 2.

One can easily check that if $\beta^i = 45°$ then coefficients b_S and b_B in Eq. (5) have the values of 0.155 and 0.837, respectively, which are less than 9% difference from the values shown in Ref. [7]. It should be noted that the factor b_S of Eq. (5) increases with increasing incident angles of Ar atom beams. The same effect was also noted by Agrawal and Raff [13].

Correlation of the normalized root mean square deviation of scattered atom's velocities with parameters of incidence shown in Fig. 5 can be approximated by Eq. (6) and the coefficients $A1_{n,k}$ are listed in Table 3.

$$\sigma\mu_V = f(E^i, \beta^i) = \sum_{k=0}^{7} \left\{ \sum_{n=0}^{5} \{A1_{n,k} \cdot (\beta^i)^n\} \cdot (E^i)^k \right\} \tag{6}$$

Both polar and azimuthal angles of the scattered atoms were varied within ranges of $[-\pi/2; \pi/2]$, thus the normalized RMSD corresponding to a uniform distribution for random numbers within this range was [14]:

$$\sigma_{uni} = \frac{b-a}{\sqrt{12}} = \frac{180}{\sqrt{12}} = 30\sqrt{3} \tag{7a}$$

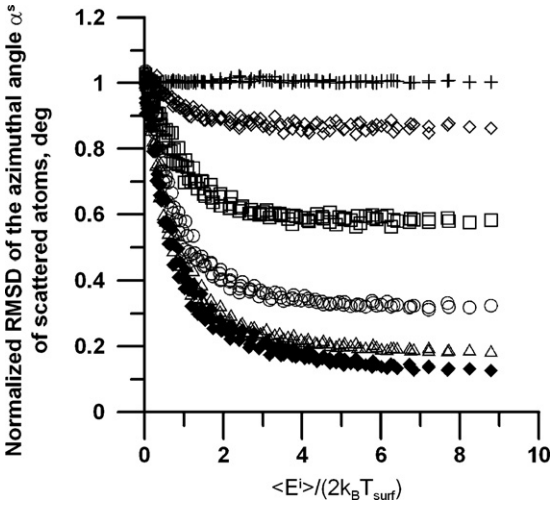

Fig. 6. Normalized root mean square deviation σ_α of the azimuthal angle α^s of scattered atoms versus kinetic energy of impinging atoms and incident polar angle. +, $\beta^i = 0°$; ◊, $\beta^i = 15°$; □, $\beta^i = 30°$; ○, $\beta^i = 45°$; Δ, $\beta^i = 60°$; ♦, $\beta^i = 70°$.

Thus, the normalized RMSDs of scattering of the scattering angles α^s and β^s, respectively, are defined as follows:

$$\overline{\sigma_\alpha} = \frac{\sigma_\alpha}{\sigma_{uni}} = \frac{\sigma_\alpha}{30\sqrt{3}} \tag{7b}$$

$$\overline{\sigma_\beta} = \frac{\sigma_\beta}{\sigma_{uni}} = \frac{\sigma_\beta}{30\sqrt{3}} \tag{7c}$$

RMSDs of the scattering angles α^s and β^s as presented in Figs. 6 and 7, respectively, were normalized by the σ_{uni} from Eq. (7a). Based on the results shown in Fig. 6, one could conclude that the mean azimuthal angle of the scattered beam α^s was independent of incident kinetic energy and incident angle β^i when an

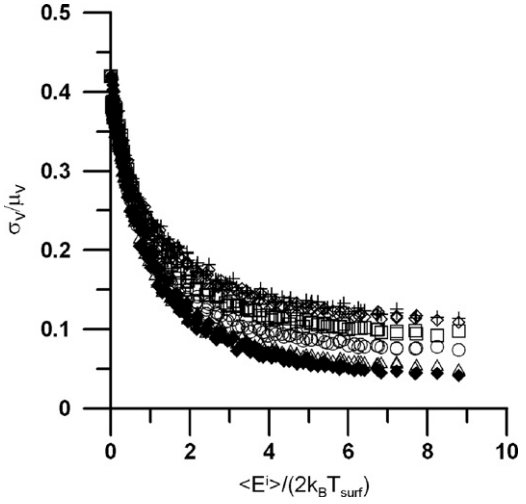

Fig. 5. Root mean square deviation of scattered atom's velocities σ_V over mean velocity of scattered atoms μ_V versus kinetic energy impinging atoms. +, $\beta^i = 0°$; ◊, $\beta^i = 15°$; □, $\beta^i = 30°$; ○, $\beta^i = 45°$; Δ, $\beta^i = 60°$; ♦, $\beta^i = 70°$.

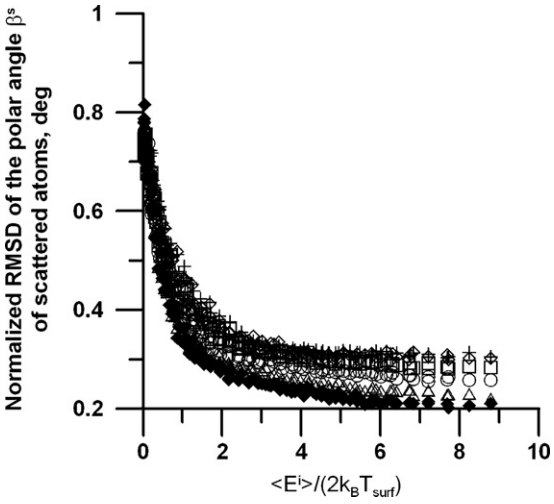

Fig. 7. Normalized root mean square deviation σ_β of the polar angle β^s of scattered atoms versus kinetic energy of impinging atoms and incident polar angle. +, $\beta^i = 0°$; ◊, $\beta^i = 15°$; □, $\beta^i = 30°$; ○, $\beta^i = 45°$; Δ, $\beta^i = 60°$; ♦, $\beta^i = 70°$.

Table 2
Coefficients $A0$ and $B0$ of the approximation polynomial (5).

k	0	1	2	3	4	5
$A0_k$	0.7657	$-8.5557*10^{-5}$	$5.4918*10^{-5}$	$-4*10^{-7}$	–	–
$B0_k$	0.14	$1.183*10^{-4}$	$3.1536*10^{-5}$	$-1.963*10^{-6}$	$4.44*10^{-8}$	$-3.1069*10^{-10}$

Table 3
Coefficients $A1_{n,k}$ of the approximation polynomial (6).

n	k							
	0	1	2	3	4	5	6	7
0	4.0808E−01	−3.1798E−01	2.2149E−01	−9.4382E−02	2.3375E−02	−3.2682E−03	2.3874E−04	−7.0729E−06
1	−1.8143E−04	−3.2165E−03	5.0261E−03	−2.8516E−03	8.1348E−04	−1.2525E−04	9.9072E−06	−3.1471E−07
2	−6.2076E−05	6.3264E−04	−9.3310E−04	5.3339E−04	−1.5349E−04	2.3666E−05	−1.8628E−06	5.8677E−08
3	4.0415E−06	−3.1700E−05	4.4018E−05	−2.4904E−05	7.1564E−06	−1.1032E−06	8.6781E−08	−2.7304E−09
4	−8.7349E−08	5.8999E−07	−8.0211E−07	4.5289E−07	−1.3024E−07	2.0087E−08	−1.5799E−09	4.9678E−11
5	6.1889E−10	−3.7420E−09	5.0384E−09	−2.8462E−09	8.1957E−10	−1.2649E−10	9.9487E−12	−3.1269E−13

atom's beam impinged normally on the surface (data points represented by cross symbols). Fig. 7 presents correlation similar to those shown in Fig. 6, but for the polar angle β^s of the scattered beam.

Normalized RMSDs of the azimuthal angle α^s and polar angle β^s of scattered atoms versus kinetic energy of impinging atoms and incident polar angle shown in Figs. 6 and 7 are approximated by the polynomials (8) and (9), respectively:

$$\overline{\sigma_\alpha} = f(E^i, \beta^i) = \sum_{k=0}^{7} \left\{ \sum_{n=0}^{7} \{A2_{n,k} \cdot (\beta^i)^n\} \cdot (E^i)^k \right\} \quad (8)$$

$$\overline{\sigma_\beta} = f(E^i, \beta^i) = \sum_{k=0}^{7} \left\{ \sum_{n=0}^{5} \{A3_{n,k} \cdot (\beta^i)^n\} \cdot (E^i)^k \right\} \quad (9)$$

It is obviously from Fig. 7 that the RMSD of polar angle of scattered atoms is inversely proportional to the incident energy, i.e., the angular distribution becomes narrower while the incident energy increases. Fig. 8 shows that fraction of atoms scattered in backward direction is sufficient in case of low incident energy Ar atoms and it decreases when the energy of falling beam becomes higher. These conclusions are in line with experimental results shown in Refs. [15,16].

Coefficients $A2_{n,k}$ and $A3_{n,k}$ for Eqs. (8) and (9) are listed in Tables 4 and 5, respectively.

Fig. 9 illustrates the correlation of the average polar angle β^s of the scattered atoms with incident kinetic energy and polar angle β^i. This is approximated by the polynomial Eq. (10) having coefficients $A4_{n,k}$ which are listed in Table 6.

$$\mu_\beta = f(E^i, \beta^i) = \sum_{k=0}^{2} \left\{ \sum_{n=0}^{12} \{A4_{n,k} \cdot (E^i)^n\} \cdot (\beta^i)^k \right\} \quad (10)$$

The results presented in Fig. 8 shows that an increase in incident energy caused linearization of dependence between the incident and the scattered polar angle, while the average polar angle of the scattered argon atoms that had low incident energy tended toward zero. Correlation coefficient between average value of polar angle β^s of scattered atoms and incident angle β^i of the beam is shown in Fig. 10. Fig. 10 proves that correlation between angles mentioned above becomes linear when the incident energy is high enough.

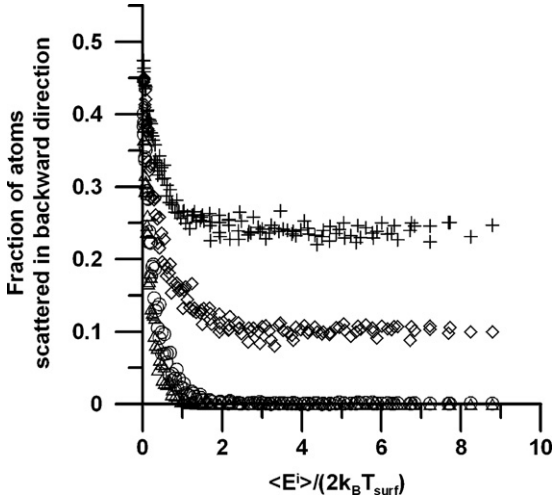

Fig. 8. Fraction of atoms scattered in backward direction versus energy of impinging Ar atoms. +, $\beta^i = 10^\circ$; ◊, $\beta^i = 20^\circ$; ○, $\beta^i = 40^\circ$; Δ, $\beta^i = 60^\circ$.

It is clear that the distribution of the angle β^s did not become fully uniform (the angle did not become independent of other parameters) in the range of studied incident parameters of Ar beam. On the other hand, the distribution of the angle α^s became uniform (as shown by the cross symbols in Fig. 11) when the incident beam had low energy ($\langle E^i \rangle / (2k_B T_{surf}) \approx 0$) or was a normal falling beam ($\beta^i \approx 0$), and became Gaussian when the incidents had high

Table 4
Coefficients $A2_{n,k}$ of the approximation polynomial (8).

n	k							
	0	1	2	3	4	5	6	7
0	1.0712E+00	7.3238E−02	−8.8442E−02	5.2060E−02	−1.6027E−02	2.6247E−03	−2.1649E−04	7.0685E−06
1	−2.0793E−03	1.0793E−02	−2.0503E−02	1.0220E−02	−2.2900E−03	2.5026E−04	−1.2243E−05	1.7791E−07
2	8.6448E−04	−8.6467E−03	1.0127E−02	−5.0983E−03	1.3124E−03	−1.8107E−04	1.2747E−05	−3.5960E−07
3	−9.8449E−05	7.6928E−04	−9.0643E−04	4.6986E−04	−1.2515E−04	1.7885E−05	−1.3046E−06	3.8140E−08
4	4.5169E−06	−3.1373E−05	3.7164E−05	−1.9772E−05	5.4091E−06	−7.9247E−07	5.9136E−08	−1.7658E−09
5	−1.0050E−07	6.5031E−07	−7.7981E−07	4.2601E−07	−1.1940E−07	1.7857E−08	−1.3563E−09	4.1131E−11
6	1.0868E−09	−6.6825E−09	8.1503E−09	−4.5652E−09	1.3062E−09	−1.9861E−10	1.5291E−11	−4.6908E−13
7	−4.5898E−12	2.7098E−11	−3.3664E−11	1.9270E−11	−5.6071E−12	8.6358E−13	−6.7172E−14	2.0781E−15

Table 5
Coefficients $A3_{n,k}$ of the approximation polynomial (9).

n	k							
	0	1	2	3	4	5	6	7
0	7.6831E−01	−5.5235E−01	3.5233E−01	−1.3976E−01	3.3855E−02	−4.7690E−03	3.5569E−04	−1.0811E−05
1	−1.0661E−03	−2.6447E−03	4.3213E−03	−1.8036E−03	2.6667E−04	−1.7706E−06	−2.7154E−06	1.6567E−07
2	1.0522E−04	3.7658E−05	−2.0959E−04	1.1142E−04	−2.1592E−05	1.2882E−06	6.5481E−08	−7.1913E−09
3	−3.4014E−06	−7.3489E−06	1.4560E−05	−7.7702E−06	1.8641E−06	−2.1876E−07	1.1619E−08	−1.9147E−10
4	4.5134E−08	1.7438E−07	−3.0241E−07	1.6259E−07	−4.1163E−08	5.3403E−09	−3.3836E−10	8.0756E−12
5	−1.9840E−10	−1.1959E−09	1.9698E−09	−1.0674E−09	2.7775E−10	−3.7634E−11	2.5370E−12	−6.6354E−14

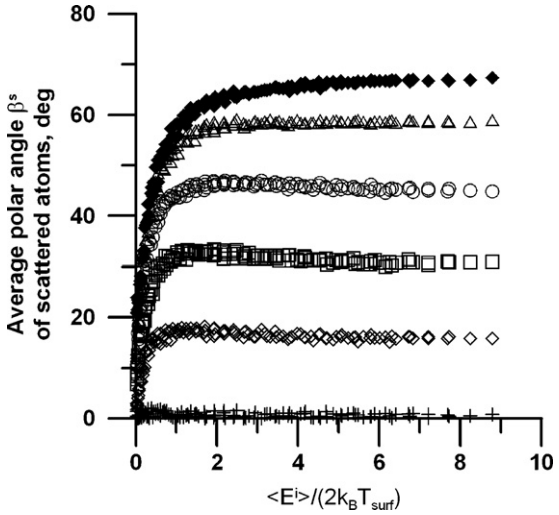

Fig. 9. Average polar angle β^s of scattered atoms versus kinetic energy of impinging atoms and incident polar angle. +, $\beta^i = 0°$; ◊, $\beta^i = 15°$; □, $\beta^i = 30°$; ○, $\beta^i = 45°$; Δ, $\beta^i = 60°$; ♦, $\beta^i = 70°$.

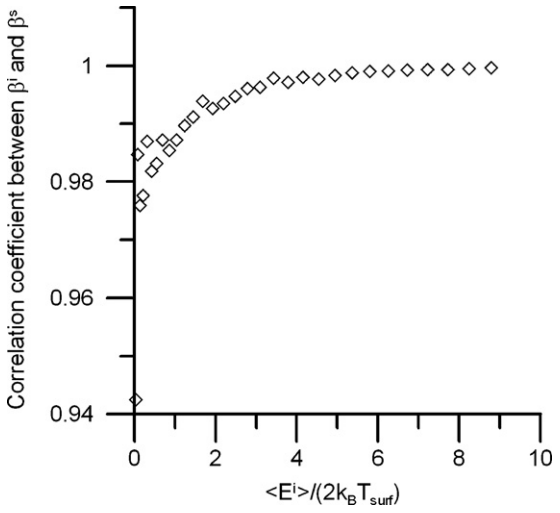

Fig. 10. Correlation coefficients between β^i and β^s versus energy of incident beam.

energy (shown as crosses and a dashed line in Fig. 12). Comparing angle β^s in Figs. 11 and 12, one can see that the scattering of Ar atoms was more specular in the case of the high energy falling beam (Fig. 12) than in the case of the low energy one (Fig. 11). It should be noted that scattering does not become fully specular in the range of studied parameters, because Ar atoms change their energy and momentum upon collision. This issue can also be explained in terms of relation between E^i_{min} and ε_{WAr}.

Probability distribution functions (PDF) presented in Figs. 11 and 12 have 30 bins and the critical value of Chi-square corresponding to 0.05 level of significance is 42.56. Values of χ^2 for the curves fitting the data points presented in Fig. 11 are 9.18 and 13.01, corresponding to uniform PDF of α^s and normal distribution of β^s, respectively. The values of χ^2 for functions fitting the distributions of angles α^s and β^s of scattered atoms are 11.13 and 12.94, respectively. All these values do not exceed the critical value of the Chi-square. It means that these distribution functions can fit data points well.

By summarizing the results and discussion above, a new algorithm for better describing the scattering behaviors of argon atoms on tungsten surface is proposed:

1. Parameters β^i, α^i, V^i are to be determined from gas atom velocity components that reached stated boundary;
2. Parameters μ_V, σ_V, σ_α, σ_β, and μ_β were determined by using Eqs. (5), (6) and (8)–(10), respectively;

Table 6
Coefficients $A4_{n,k}$ of the approximation polynomial (10).

n	k		
	0	1	2
0	5.0233E−01	9.3434E−02	1.4669E−03
1	−8.7760E−01	5.1610E+00	−4.5275E−02
2	5.0029E+00	−1.0590E+01	1.0505E−01
3	−1.1770E+01	1.2610E+01	−1.3069E−01
4	1.3326E+01	−9.4402E+00	9.9784E−02
5	−8.6626E+00	4.6457E+00	−4.9576E−02
6	3.5302E+00	−1.5475E+00	1.6589E−02
7	−9.4203E−01	3.5421E−01	−3.8039E−03
8	1.6723E−01	−5.5725E−02	5.9857E−04
9	−1.9580E−02	5.9177E−03	−6.3514E−05
10	1.4527E−03	−4.0511E−04	4.3416E−06
11	−6.1898E−05	1.6135E−05	−1.7258E−07
12	1.1538E−06	−2.8400E−07	3.0305E−09

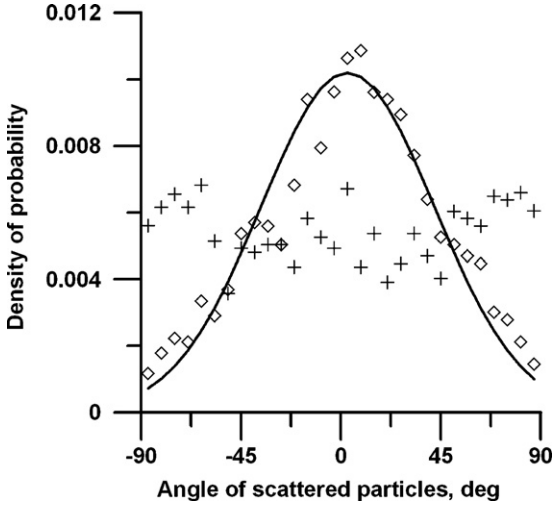

Fig. 11. Density of probability of β^s and α^s. $T_{surf} = 350$ K, $\beta^i = 20°$, $V^i = 100$ m/s. +, distribution of α^s; ◊, distribution of β^s; solid line – normal distribution of β^s.

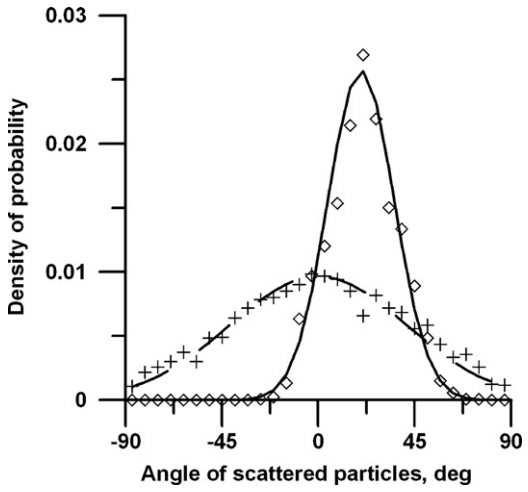

Fig. 12. Density of probability of β^s and α^s. T_{surf} = 350 K, β^i = 20°, V^i = 1500 m/s. +, distribution of α^s; ◊, distribution of β^s; solid line – normal distribution of β^s; dashed line – normal distribution of α^s.

3. If $\sigma_\alpha \geq 0.9$ then angle α is to be determined by using a random function with uniform distribution, otherwise α should be determined by using a sampling method based on the Gaussian probability function with the RMSD value obtained in step 2 and mean value equal to 0. α^s of the scattered atoms is then defined as $\alpha^s = \alpha + \alpha^i$.
4. Parameter β^s was defined by using a sampling method based on the normal probability function with the RMSD σ_β value obtained in step 2 and mean values equal to the μ_β of β^s.
5. The velocity of the scattered atom V^s is to be defined by using a sampling method based on Maxwell distribution and mean value μ_V when the incident atom's energy was $\langle E^i \rangle / (2k_B T_{surf}) \leq 1$, and by using the normal probability function with the RMSD σ_V value obtained in step 2 and mean value μ_V otherwise.

The presented algorithm was tested by replacing the tungsten substrate with a flat surface having a temperature of T_{surf} = 350 K and T_{surf} = 500 K and applying new BCs described by the above-mentioned algorithm. We found that the proposed model was capable of reproducing the processes of the interaction between argon atoms and the tungsten substrate described above. It should be noted that computation time by use of this algorithm is only one-twelfth of computation time of MD simulation involving the real tungsten substrate. It is obvious that the amount of time saving will rise proportionally to the scale of solid surfaces reproduced by using the algorithm mentioned above.

4. Conclusion

In this work we developed new boundary conditions which are able to reproduce the behaviors of argon atoms interactions with tungsten surface. The new proposed boundary conditions are based on Gaussian, uniform and Maxwellian probability distribution functions conducted together by using a set of polynomial functions. Such approach made this model of boundary condition more flexible and realistic compared with the simple specular-diffusive one. In the previous section we have proposed an algorithm to describe how the polynomial and probability distribution functions mentioned above could be used as boundary conditions. Generally, this works explains how to implement normalization and further conversion of the experimental or simulation results into boundary conditions.

Application of the new proposed boundary conditions for Ar–W interactions is proven to be able to significantly speed up computations. The computation time by use of this algorithm is only about one-twelfth of computation time of MD simulation involving the real tungsten substrate. This is implemented by replacement of atoms on solid surfaces with surfaces following the gas scattering law described by the new boundary conditions.

Acknowledgments

The authors would like to acknowledge the kind funding support from NSC Taiwan under the contracts of NSC 101-2923-E-006-001-MY3 and NSC 99-2923-E-006-006-MY3.

References

[1] S. Varoutis, D. Valougeorgis, O. Sazhin, F. Sharipov, Rarefied gas flow through short tubes into vacuum, Journal of Vacuum Science and Technology A: Vacuum, Surfaces, and Films 26 (2) (2008) 228–238.
[2] F. Sharipov, Rarefied gas flow through a long tube at any temperature ratio, Journal of Vacuum Science and Technology A: Vacuum, Surfaces, and Films 14 (4) (1996) 2627–2635.
[3] S. Varoutis, D. Valougeorgis, F. Sharipov, Simulation of gas flow through tubes of finite length over the whole range of rarefaction for various pressure drop ratios, Journal of Vacuum Science and Technology A: Vacuum, Surfaces, and Films 27 (6) (2009) 1377–1391.
[4] J.C. Maxwell, On stresses in rarified gases arising from inequalities of temperature, Philosophical Transactions of the Royal Society of London 170 (1879) 231–256.
[5] T.-S. Leu, C.-H. Cheng, M.S. Ozhgibesov, New modeling of scattering behaviors of argon atoms on tungsten substrate, Journal of Molecular Graphics and Modelling 31 (2011) 35–40.
[6] W.H. Weinberg, R.P. Merrill, Scattering of helium, neon, argon, krypton, xenon, and deuterium from a tungsten (1 1 0) surface characterized by LEED, The Journal of Chemical Physics 56 (6) (1972) 2881–2892.
[7] K.C. Janda, J.E. Hurst, C.A. Becker, J.P. Cowin, D.J. Auerbach, L. Wharton, Direct measurement of velocity distributions in argon beam–tungsten surface scattering, The Journal of Chemical Physics 72 (4) (1980) 2403–2410.
[8] G. Fan, J.R. Manson, Theory of direct scattering, trapping, and desorption in atom–surface collisions, Physical Review B 79 (4) (2009) 045424.
[9] K.D. Gibson, N. Isa, S.J. Sibener, Experiments and simulations of Ar scattering from an ordered 1-decanethiol–Au(1 1 1) monolayer, The Journal of Chemical Physics 119 (24) (2003) 13083.
[10] S. Maruyama, Molecular dynamics method for microscale heat transfer, Advances in Numerical Heat Transfer 2 (2000) 189–226.
[11] G.A. Bird, Molecular Gas Dynamics and the Direct Simulation of Gas Flows, Clarendon Press, Oxford University Press, Oxford, New York, 1994.
[12] A. Papoulis, Probability, Random Variables, and Stochastic Processes, 3rd ed., McGraw-Hill, New York, 1991.
[13] P.M. Agrawal, L.M. Raff, A semiclassical wave packet model for the investigation of elastic and inelastic gas–surface scattering, The Journal of Chemical Physics 77 (8) (1982) 3946–3952.
[14] R.E. Walpole, Probability & Statistics for Engineers & Scientists, 8th ed., Pearson Prentice Hall, Upper Saddle River, NJ, 2007.
[15] L. Tribe, M. Manning, J.A. Morgan, M.D. Stephens, W.R. Ronk, E. Treptow, et al., Argon scattering off the surface of liquid indium: exit angle and energy dependence, The Journal of Physical Chemistry B 102 (1) (1998) 206–211.
[16] D. Chase, M. Manning, J.A. Morgan, G.M. Nathanson, R.B. Gerber, Argon scattering from liquid indium: simulations with embedded atom potentials and experiment, The Journal of Chemical Physics 113 (20) (2000) 9279–9287.